Refined and simplified modelling of steel-concrete-steel (SCS) composite beams

R. Calixte, Luc Davenne, Ludovic Jason

Computational Modelling of Concrete and Concrete Structures – Meschke, Pichler & Rots (Eds)

Refined and simplified modelling of steel-concrete-steel (SCS) composite beams

R. Calixte
UPL, Univ Paris Nanterre, LEME – Laboratoire Energétique, Mécanique, Electromagnétisme, Ville d'Avray, France
Université Paris-Saclay, CEA, Service d'Études Mécaniques et Thermiques, Gif-sur-Yvette, France

L. Davenne
UPL, Univ Paris Nanterre, LEME – Laboratoire Energétique, Mécanique, Electromagnétisme, Ville d'Avray, France

L. Jason
Université Paris-Saclay, CEA, Service d'Études Mécaniques et Thermiques, Gif-sur-Yvette, France

ABSTRACT: This study presents a general simulation methodology to assess both full and partial composite action of steel-concrete-steel (SCS) structures. This refined methodology, using 3D finite elements, is applied to two three-point bending beams in which a different composite action is provided through variation of the number of studs. The comparison to experimental results validates the methodology and the global and local behavior can be reproduced. However, the important calculation cost reduces the use of this numerical strategy to more complex structures. A simplified methodology is proposed with 1D finite elements to represent the connectors. This modelling choice allows to greatly reduce the computational cost. It also imply a reduction of the reproduced phenomena. Particularly, local damage of the concrete core around the dowels is slightly different. Nevertheless, this strategy allows to accurately reproduce the global behavior as well as the failure modes of SCS beams with full and partial composite action.

1 INTRODUCTION

The Strength, stiffness and durability requirement for civil engineering constructions are steadily increasing. To fulfil these new needs, studies are launched to develop new structural materials with higher specifications. Steel-concrete-steel (SCS) composite structures are one of them (Leekitwattana et al. 2010; Leng & Song 2016; Varma et al. 2015). This composite structure is composed of a concrete core caught between two steel plates. The bond between the components is made thanks to a connection system, generally performed through steel dowels and/or ties (Figure 1). This component is responsible for composite action and ensures the overall behavior of the SCS structure. The structure thus composed has the advantages of reinforced concrete like a good strength and stiffness thanks to the optimal use of the concrete and of the steel. Moreover, the external place of the steel plate increases the stiffness, the sustainability, and the strength under some extreme solicitations (Booth et al. 2015; Bowerman et al. 2002; Oduyemi & Wright 1989; Yan et al. 2015). It also allows their use as lost formwork, which can be prefabricated and SCS are modular structures (Leekitwattana et al. 2010; Schlaseman 2004; Varma et al. 2015). SCS structures structures have been gradually used in bridge deck (Yan et al. 2015), for the construction of shear walls in high buildings (AISC 2017), for submerged tunnels (Calatrava 2013; Bekarlar 2016) and for blast and impact shield walls or liquid and gas containers (Wright et al. 1991, Liew et al. 2016).

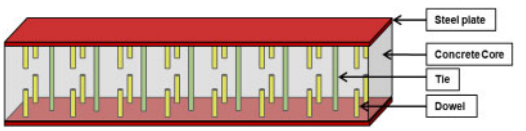

Figure 1. Geometry of a SCS beam with dowels and ties.

The study of bending beams allows to better understand the behavior of this type of structural material. With this aim, the number of research on SCS beams has increased since 1975 (Montague 1975). Several behaviors have been identified depending on the geometric and material characteristics of the structures (Sener et al. 2016; Wright et al. 1991; Yan et al. 2014). Particularly, depending on the degree of composite action, the SCS beam present a full or a partial composite action. Directly affected by the number of connectors, the difference of composite action will

DOI 10.1201/9781003316404-40

impact the global behavior and the failure mode of the structure (Dogan & Roberts 2010; Zhang et al. 2020). The study of both types of behavior is necessary to consider all scenarios, such as design and construction choices, loss of structural integrity or construction difficulties, among others (Lin et al. 2019; Qin et al. 2015; Zhang et al. 2020).

2 MODELING STRATEGY

In this section, a numerical methodology is proposed to represent both full and partial composite actions in SCS structures. It is applied on two representative three-point bending beams.

2.1 *Experiment*

The SP1-1 and SP1-2 beams of the experimental study of Sener et al. (2016) are considered. They have the same geometry (Figure 2 and Table 1) but include a different number of welded headed shear studs. The beams are loaded in three-point bending (simply supported with a load applied at the mid-span). The applied load, the vertical displacements under the loading point, and the cracking evolution are experimentally monitored.

The experimental material properties are given in Tables 2 and 3.

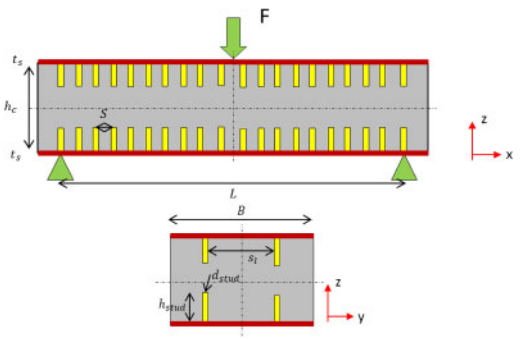

Figure 2. Geometry of SP1 beam.

Table 1. Geometrical parameters of SP1-1 and SP1-2 beams.

	Symbol	SP1-1	SP1-2
Nr of dowels per steel plate	n_{stud}	40	20
Spacing of dowels (length)	S (mm)	152.4	304.8
Length of beam	L (mm)	2896	
Width of beam	B (mm)	305	
Thickness of steel plates	t_s (mm)	6.5	
Height of concrete core	h_c (mm)	445	
Diameter of dowels	d_{stud} (mm)	12.7	
Height of dowels	h_{stud} (mm)	63.5	
Spacing of dowels (width)	sl (mm)	152	

Table 2. Concrete properties.

Compressive strength	f_c (MPa)	42
Tensile strength*	f_{ct} (MPa)	3.15
Young modulus*	E_c (GPa)*	33.85
Poisson's ratio*	ν_c (–)	0.2

* Obtained with Eurocode 2 (CEN 2004a) formulas

Table 3. Steel properties.

		Plates	Dowels
Yield limit	f_y (MPa))	448	489
Young modulus	E_s (GPa)	201	201
Hardening modulus	E_T (GPa)	0.42	0.42
Poisson's ratio	ν_s (–)	0.3	0.3

2.2 *Material behavior modeling*

Concrete behavior is simulated using an isotropic damage model based on Mazars' model (Mazars 1984) with a regularized damage evolution in tension and in compression through the Hillerborg et al. (1976) method. This law introduces a scalar variable D that quantifies the influence of microcracking:

$$\sigma_{ij} = (1 - D) C_{ijkl} \varepsilon_{kl} \tag{1}$$

where σ_{ij} and ε_{kl} are respectively the stress and strain components, respectively, C_{ijkl} is the fourth order elastic tensor and D is the damage variable. For the description of the damage growth, an equivalent strain is introduced from the local strain tensor:

$$\varepsilon_{eq} = \sqrt{\sum_{i=1}^{3} (< \varepsilon_i >_+)^2} \tag{2}$$

where $<\varepsilon_i>_+$ are the positive principal strains.

The loading surface g is defined by:

$$g(\varepsilon, D) = \tilde{d}(\varepsilon) - D \tag{3}$$

where the damage variable D is also the history variable which takes the maximum value reached by $\tilde{d}$ during the history of loading

$$D = \max(\tilde{d}, 0) \tag{4}$$

$\tilde{d}$ is defined by an evolution law which distinguishes the mechanical responses of the material in tension and in compression by introducing two scalars D_t and D_c.

$$\tilde{d}(\varepsilon) = \alpha_t(\varepsilon) D_t(\varepsilon_{eq}) + \alpha_c(\varepsilon) D_c(\varepsilon_{eq})$$

$$D_t = 1 - \frac{\kappa_0}{\varepsilon_{eq}} \exp\left(\frac{l_e . f_{ct}}{G_F}(\kappa_0 - \varepsilon_{eq})\right)$$

$$D_c = 1 - \frac{\kappa_0 (1 - A_c)}{\varepsilon_{eq}} - \frac{A_c}{\exp\left[B_c (\varepsilon_{eq} - \kappa_0)\right]} \tag{5}$$

$$\alpha_{t,c} = \left(\sum_{i=1}^{3} \frac{< \varepsilon_i^{t,c} > < \varepsilon_i >_+}{\varepsilon_{eq}^2} \right)^{\beta}$$

D_t and D_c are the tensile and compressive parts of the damage, respectively. The weights α_t and $\alpha_c$are computed from the strain tensor. They are defined as functions of the principal values of the strains $\varepsilon_{ij}^t$and ε_{ij}^c due to positive and negative stresses respectively. The parameter β reduces the effect of damage under shear compared to tension. For the regularization in tension, D_t involves l_e, the average size of the finite element (cubic root of the element volume), G_F the fracture energy and f_{ct} the tensile strength. κ_0 is a parameter (equal to the ratio between the tensile strength and the Young's modulus) and represents the initial threshold from which damage grows. A_c and B_c are two parameters for the compression damage evolution. For the regularization in compression, they are calibrated from uniaxial compression simulations to obtain the same stress – displacement curve for different values of element size l_e. The calibration process is thus based on a constant compressive cracking energy concept, as defined by van Mier 1984.

$$D_c = 1 - \frac{\kappa_0 (1 - A_c)}{\varepsilon_{eq}} - \frac{A_c}{\exp\left[B_c \left(\varepsilon_{eq} - \kappa_0\right)\right]} \qquad (6)$$

The Kuhn – Tucker conditions finally determines the evolution of damage:

$$g \leq 0, \quad \dot{d} \geq 0, \quad g\dot{d} = 0 \qquad (7)$$

From the experimental data resumed in Table 2 the model parameters in Table 4 are chosen to reproduce the concrete behavior.

Table 4. Concrete model parameters.

$\boldsymbol{A_c}$	$68l_e^2 + 19l_e$	*
$\boldsymbol{B_c}$	$26000l_e + 1$	*
$\boldsymbol{G_F}$ (J·m^{-2})	150	
$\boldsymbol{\kappa_0}$	9.31 10^{-5}	
$\boldsymbol{\beta}$	0.6	

* For l_e in m

For the steel plates and the steel dowels, an elastic plastic behavior with an isotropic hardening is chosen.

To be able to capture the shear failure of the dowel, an extremely refined mesh would be required in the plate-stud interface area, leading to very high computational costs. To avoid this, zero-dimension junction elements are used, connecting each stud node to the associated plate node. Their force-displacement law is elastoplastic in the tangential direction, with a very stiff elastic part ($K_s = 10^{12} N/m$). Each junction element has a yield limit proportional to the area attached to the node. The sum of the yield limits of the junction elements is equal to the shear failure of the stud P_{Rd} which is calculated as in the Eurocode 4 (CEN 2004b) without the safety factor:

$$P_{Rd} = 0,8 f_y A_{stud} = 49.5kN \qquad (8)$$

2.3 *Refined numerical modelling*

Considering the symmetries, only one fourth of the beams are modelled (Figure 3 and Figure 4). The size of the concrete finite elements ranges from 1.6 mm (near the dowels connector) to 25 mm (far from the connectors).

Given the expected behavior of the structure, a particular attention is paid to the bond between concrete and steel (Figure 5). A one-sided contact relationship is considered between steel plates and concrete, that allows for normal separation and a free slip in the tangential directions (partial bond). The same condition is applied between concrete and dowels. The stud heads are not meshed in detail. A simple perfect bond is imposed at the end of each dowel.

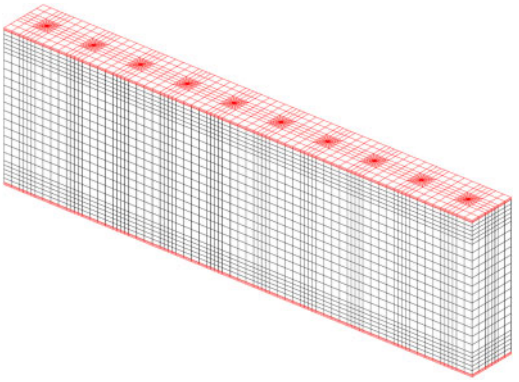

Figure 3. Mesh of SP1-1 beam.

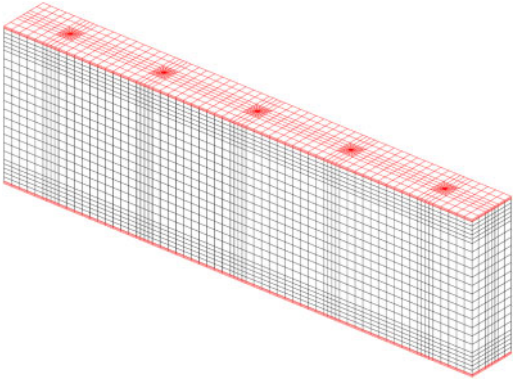

Figure 4. Mesh of SP1-2 beam.

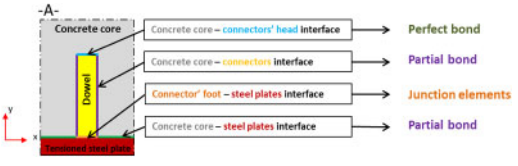

Figure 5. Interfacial bonds between steel and concrete.

The global boundary conditions on the beam are symmetry conditions and displacement in the vertical direction blocked along lines at the position of the experimental support (Figure 6). Finally the loading is imposed through a vertical displacement applied on the upper steel plate at the position of the experimental loading system.

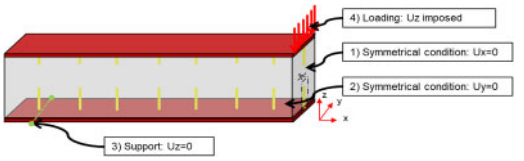

Figure 6. Boundary conditions on the beam.

The simulations are performed using the implicit finite element code Cast3M (CEA 2021).

3 NUMERICAL SIMULATIONS

3.1 *SP1-1 beam*

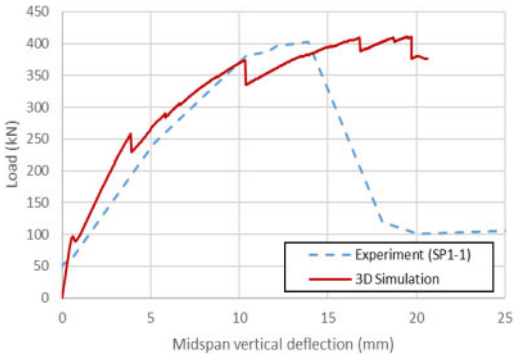

Figure 7. Load – midspan vertical displacement curves for the SP1-1 beam.

Figure 7 presents the global response of SP1-1 beam.

The general mechanical behavior is obtained by the simulation (elastic regime and mechanical degradation). The structural strength is reproduced. For a 13.9 mm deflection (the one of the experimental ruin), the strength obtained with the 3D simulation is 382.02 kN, 6% different of the experimental result. Several partial discharges are observed in the numerical curve. The first one corresponds to the initiation of the vertical flexural crack. As for the test, this crack appears quickly and modifies the stiffness of the structure. The second unloading represents the opening of the 45° inclined concrete shear crack. This crack appears for an applied force of 258 kN. The following discharge corresponds to the opening of concrete cracks in the lower part of the beam, illustrating the propagation of damage parallel to the bottom plate.

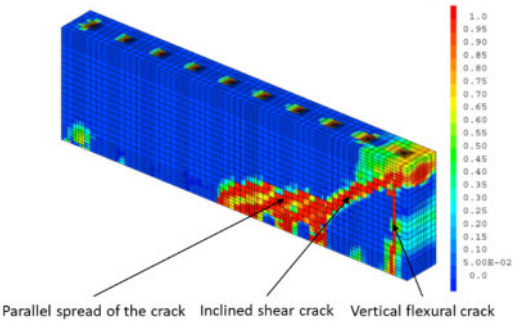

Figure 8. Final damage distribution in concrete for the SP1-1 beam.

Figure 9. Experimental final crack pattern for SP1-1 beam.

The damage distribution obtained in the simulation (Figure 8) is like the experimental crack pattern (Figure 9). The experimental and numerical longitudinal strains in the steel plates are also in agreement (Figure 10). A local yielding of the bottom steel plate is observed near the position of the shear crack feet for the numerical simulation. For the experimental results, this yielding is visible in the right span of the beam, at the same distance of the midspan. It is to be noted that the pic of strain in the top steel plate at the midspan for the simulation is due to the concentrated applied load (on a line).

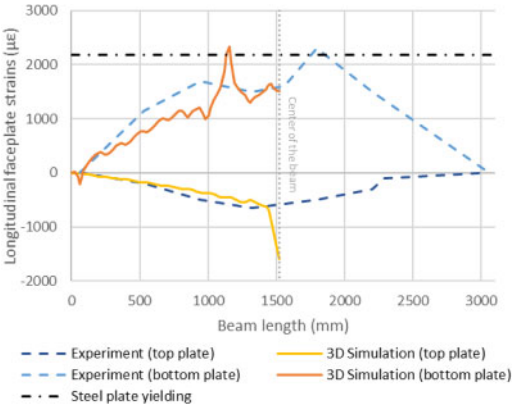

Figure 10. Longitudinal strain in the plates along SP1-1 beam for a deflection of 13.9 mm.

3.2 *SP1-2 beam*

The global mechanical behavior of SP1-2 beam is also correctly captured (Figure 11). The strength is lower (250 kN compared to 400 kN for SP1-1).

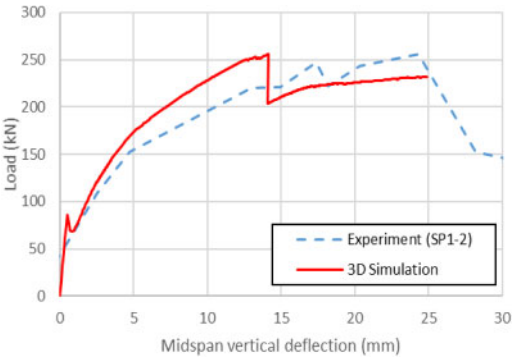

Figure 11. Load – midspan vertical displacement curves for the SP1-2 beam.

As for the SP1-1 beam, the first discharge corresponds to the initiation of a vertical flexural crack at the dowel near the midspan. The second discharge appears at a deflection of 13.9 mm and a load of 256.15 kN. This drop of load corresponds to the apparition of a shear crack inclined at more than 45° (Figure 12) which is not mentioned experiment-ally. However, Zang et al. (2020) obtained this fai-lure mode for beams with a low number of dowels.

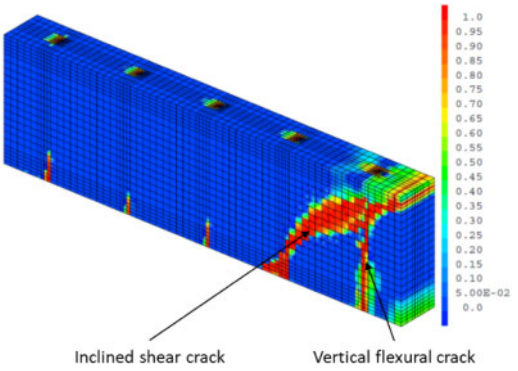

Figure 12. Final damage distribution for the SP1-2 beam.

After the peak load, a constant force is observed for an increasing displacement. Due to the yielding of the dowels, the shear force that can be transferred between the stud and the bottom steel plate has reached its maximum. This is coherent with the experimental failure due to a vertical flexural crack as seen on Figure 13. One can observe a break in the connection of the lower plate due to the failure of the studs.

Finally, the numerical curve shows a strength of the beam of 231.7 kN at a deflection of 25.4 mm (the one of the experimental ruin), less than 8% different of the experimental result.

The simulation of the longitudinal strain of the steel plate shows a slight underestimation of the bottom plate tensile strains compared to the experimental one (Figure 14).

Figure 13. Experimental failure of SP1-2 beam.

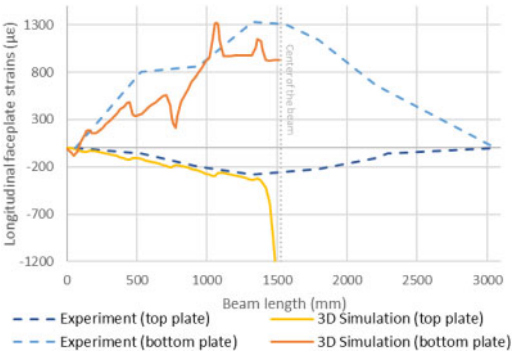

Figure 14. Longitudinal strain in the plates along SP1-2 beam for a deflection of 24.3 mm.

3.3 *Discussion*

The observed differences between experiment and simulation may be explained by some model simplifications: the contact relation without friction between the concrete core and the steel plate, the simplification of the stud heads by a perfect bond to the concrete or the simplification of the behavior of the dowel – steel plates junction elements with a perfect elastic plastic constitutive law. However, the proposed numerical methodology can reproduce the global and local behaviors for both beams. Especially, the differences between a full and a partial composite action beams are obtained: the decrease in the strength and the stiffness, the increase in the ductility and the change in the failure mode.

As the experimental results, the numerical results show a difference in strength and failure behavior between the SP1-1 and SP1-2 beams. In the first one, the number of dowels is sufficient to assure a full composite action. The connection system can support the shear force corresponding to the yielding of the bottom steel plate (Figure 10). This yielding corresponds to the ultimate strength reachable, even with a perfect bond between steel and concrete. It is to be noted that the bottom steel plate is more loaded plate due to the cracking of concrete in tension. On the contrary, in the second one, the connection system is not strong enough and is the weak link. It fails before reaching the yielding of the bottom plate, as it can be seen in Figure 14. In this case there is a partial composite action.

Based on this modeling strategy, one can perform different simulations increasing progressively the number of dowels in the beam and determine the minimum number of studs to reach a full composite action. This work has been done, including a comparison to the provisions of different design codes (Calixte 2021).

4 SIMPLIFIED MODELING

The numerical modelling strategy previously developed allows to represent finely the behavior of the composite structure connection system in shear. However, it can be costly in terms of implementation and calculation time, which reduces its use for SCS industrial structures with larger dimensions and complex geometries. To propose a less expensive numerical simulation, a 1D simplification of the connectors is studied. The representation of the connectors by one-dimensional beam finite elements anchored in the concrete will facilitate the realization of the mesh, reduce the number of nodes and elements, and simplify the interfacial conditions between the components of the system.

4.1 *Simplified modeling*

The implementation of the 1D simplification requires the modification of the interfacial bond conditions (Figure 15). A perfect bond between the concrete and the studs is imposed through kinematic conditions (Lagrange multipliers). A particular attention is paid to the concrete mesh around the studs. The 1D steel beam element nodes should be in the middle of the concrete solid element in which they are embedded, and the size of these solid elements should be near the dowel diameter dimension. For the interface between the stud and the steel plate, a 0D plastic junction element represents the bond between the stud and the steel plate. Finally, the rotation of the studs around their axis are blocked.

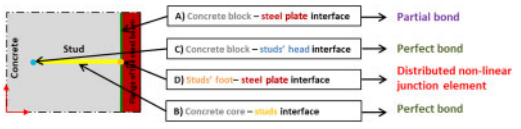

Figure 15. Interfacial bonds of the 1D simplified modelling.

Simulations on push-out tests with 1D elements for the studs showed that, compared to experimental results, the connection system modeled in this way leads to an over-rigidity of the connection behavior (Calixte 2021). The 1D modelling of the studs does not allow to reproduce finely the interactions with the concrete core because the perfect bond reduce the allowable strain of the system. On the other hand, the yield plateau of the stud – steel beam interface junction element is found, thanks to the plastic behavior of the 0D junction element at the stud foot.

To implicitly consider all the phenomena characterizing the shear response of the connection system (crushing and tearing of the concrete, shearing of the connectors, yield of the steel beam), a constitutive law reproducing of the push-out test response is adopted for the 0D junction element at the studs – steel plate interfaces. The chosen law is the one developed by Ollgaard et al. (1971) (Figure 16):

$$P = P_{Rd}\left(1 - \exp\left(-\frac{18}{25.4}\delta\right)\right)^{\frac{2}{5}} \tag{9}$$

where P_{Rd} is the shear strength of the connection in the push-out test, including the shear failure of the stud and the failure of the concrete under the pulling out of the stud:

$$P_{Rd} = \min\left(0.8 f_y A_{stud}; 0.5 A_{stud}\sqrt{f_c E_c}\right) \tag{10}$$

Calixte (2021) showed that with this nonlinear behavior for the 0D element at the dowel foot, the simulations on push-out tests gave a good agreement with the experiment in the global force - displacement response. This is evident since it is the input in the model. But the damage evolution in the concrete around the 1D stud elements is also like the one in the 3D reference simulations, which is not the case if there is no 1D elements (only 0D elements connecting directly steel plate to concrete core).

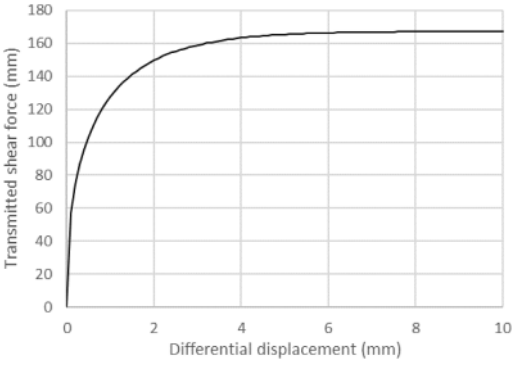

Figure 16. Ollgaard et al. (1971) push-out law.

4.2 *Numerical simulations with simplified model*

The results of the simplified modeling of SP1-1 SCS beam are presented in Figure 17 to Figure 19. The global force-displacement curve of the simplified modeling is like the one of the refined simulation (Figure 17). The difference lies in the forces where the shear crack appears, and where it propagates. The diagonal crack apparition is for a force $F = 338kN$ instead of $F = 258kN$ in the refined simulation with a 3D mesh for the dowels. The mechanical degradation is delayed in the simulation with the 1D beam elements for the dowels.

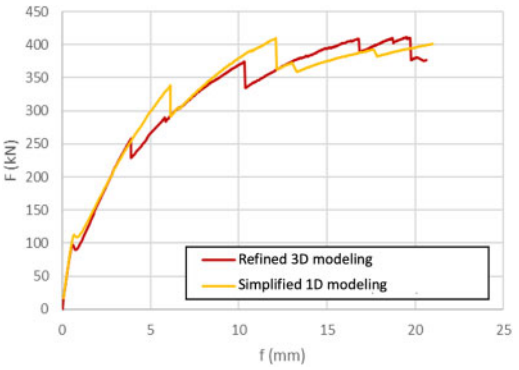

Figure 17. Displacement-force curves for SP1-1 specimen (simplified simulation).

At the end, the damage distribution for the simplified simulation is like the refined simulation one (Figure 18 compared to Figure 8). For the strains in the steel plates (Figure 19), one can see that the yielding in the bottom plate is still not reached in the 1D simulation for a displacement equal to 13.4 mm while it is for the 3D simulation. But the pic near the shear crack foot is here and yielding will soon appear.

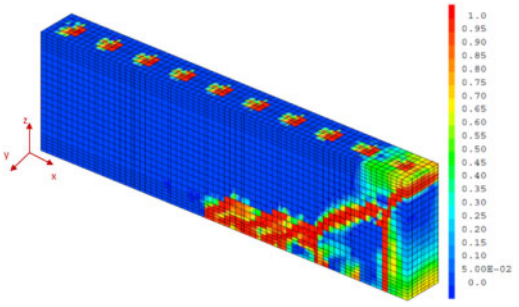

Figure 18. Final concrete damage pattern for the simplified simulation of SP1-1 specimen.

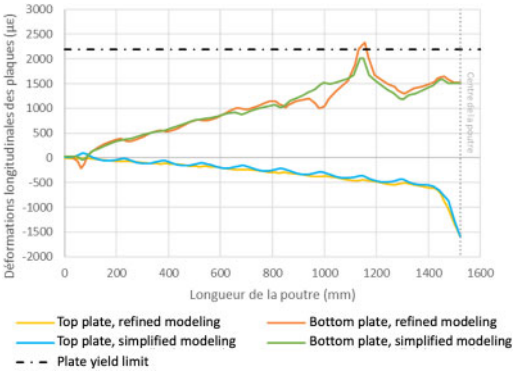

Figure 19. Longitudinal strain in the plates along SP1-1 beam for a deflection of 13.9 mm (simplified modeling simulation).

Equivalent observations are visible for the modeling of the SP1-2 beam (Figures 20 to 22). With this simplified 1D modeling, the crack inclined at more than 45° is not visible displacing the maximum longitudinal strains in the lower plate at the single vertical crack position.

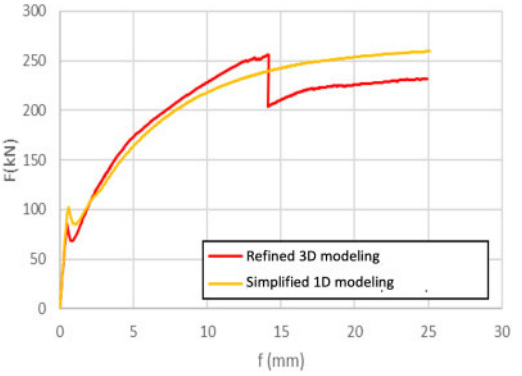

Figure 20. Displacement-force curves for SP1-2 specimen (simplified simulation).

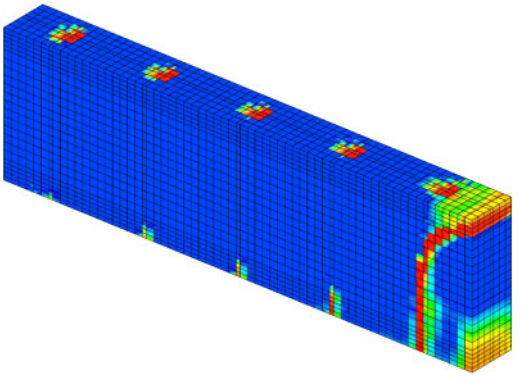

Figure 21. Final concrete damage pattern for the simplified simulation of SP1-2 specimen.

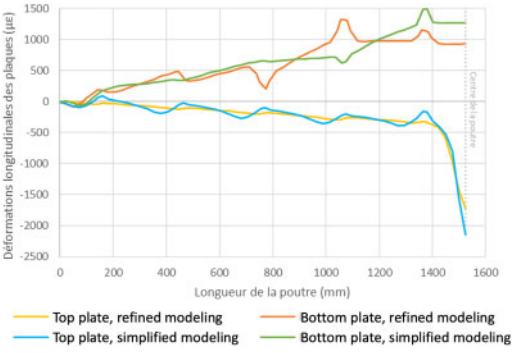

Figure 22. Longitudinal strain in the plates along SP1-2 beam for a deflection of 24.3 mm (simplified modeling simulation).

The main advantage of the simplified simulation is the time to prepare the mesh and the great gain in the computation time (Table 5).

Table 5. Comparison of calculation times.

	SP1-1		SP1-2	
	3D	1D	3D	1D
Number of nodes	51,410	17,160	34,940	15,900
Calculation time (h)	334	78	258	70

5 CONCLUSION

Steel-concrete-steel composite structures are sandwich composite structures combining steel plates and a concrete core through a connection system, which ensures the overall behavior. The structure combines the advantages of reinforced concrete and provides a greater resistance under extreme loading, sustainability, and durability. Moreover, the external position of the steel plates allows their use as formwork and leads to a modular structure, which tends to reduce and ease the construction phase. All these advantages make SCS construction a competitive choice in the construction field.

In this contribution, a general simulation methodology was proposed to assess both full and partial composite actions using 3D finite elements. It was validated by comparison to experimental results on three point bending beams. The full composite action was associated to a core concrete shear failure and a local yielding of the bottom steel plate, while the partial composite action was driven by a shear failure of the studs.

Nevertheless, the refined modeling strategy leads to significant computation times. Based on this modeling, a simplified modeling strategy with 1D elements to represent the studs has been develop-ped. The constitutive law of the junction element at the interface stud-plate includes the global law of the push-out test to implicitly consider the concrete – stud interaction not represented by this 1D modelling of the studs. Simulations with this simplified strategy led to significantly reduced computation times and the results, both in terms of global behavior and local degradation, are very similar to those obtained with the refined modeling.

ACKNOWLEDGMENTS

The authors gratefully acknowledge the financial and technical support of EDF R&D for the development and the analysis of the simulation results.

REFERENCES

AISC. 2017. Modern Steel Construction – Steel Core System Revolutionizes High-Rise Construction. *https://www.aisc.org/modernsteel/news/*

Bekarlar, K. 2016. Steel-Concrete-Steel Sandwich Immersed Tunnels For Large Spans, *Master thesis dissertation, Technische Universiteit Delft, Holland.*

Booth, P.N., Varma, A.H., Sener, K.C. & Malushte, S.R. 2015. Flexural behavior and design of steel-plate composite (SC) walls for accident thermal loading. *Nuclear Eengineering and Design* 295: 817–828. https://doi.org/10.1016/j.nucengdes.2015.07.036

Bowerman, H., Coyle, N. & Chapman, J.C. 2002. An innovative steel-concrete construction system. *Structural Engineer* 80(20): 33–38.

Calatrava 2013. Sharq Crossing – Santiago. *Calatrava Architects & Engineers https://calatrava.com/projects/*

Calixte, R. 2021. Simulation of the behavior of steel-concrete-steel structures under mechanical loading. *PhD thesis, University Paris Nanterre, France. (in French)*

CEA Commissariat à l'Energie Atomique et aux energies renouvelables. 2021. Cast3M structural and fluid mechanics calculation code. http://www-cast3m.cea.fr

CEN European Committee for Standardization. 2004a. Eurocode 2: Design of concrete structures – Part 1-1: General rules and rules for buildings. *EN 1992-1-1*

CEN European Committee for Standardization. 2004b. Eurocode 4: Design of composite steel and concrete structures – Part 1-1: General rules and rules for buildings. *EN 1994-1-1*

Dogan, O. & Roberts, T. 2010. Comparing experimental deformations of steel-concrete-steel sandwich beams with full and partial interaction theories. *International Journal of the Physical Sciences,* 5(10): 1544–1557. https://doi.org/10.1016/j.engstruct.2018.12.025

Hillerborg, A., Modéer M. & Peterson, P.E. 1976. Analysis of crack formation and crack growth in concrete by means of fracture mechanics and finite elements. *Cement and Concrete Research* 6: 773–792.

Leekitwattana, M., Boyd, S.W. & Shenoi, R.A. 2010. An alternative design of steel concrete steel sandwich beam, *9th International Conference on Sandwich Structures*, *Pasadena, United States, 14–16 June 2010.*

Leng, Y.B. & Song, X.B. 2016. Experimental study on shear performance of steel-concrete-steel Sandwich Beams, *Journal of Constructional Steel Research* 38(4): 257–279. *https://doi.org/10.1016/j.jcsr.2015.12.017*

Liew, J.Y.R., Yan J.B. & Huang Z.Y. 2016. Steel-concrete-steel sandwich composite structures – recent innovations, *Journal of constructional Steel research* 130(3): 202–221. *https://doi.org/10.1016/j.jcsr.2016.12.007*

Lin, Y., Yan, J., Wang, Y., Fan, F. & Zou, C. 2019. Shear failure mechanisms of SCS sandwich beams considering bond-slip between steel plates and concrete. *Engineering Structures* 181: 458–475. https://doi.org/10.1016/j.engstruct.2018.12.025

Mazars, J. 1984. Application de la mécanique de l'endommagement au comportement non linéaire et à la rupture du béton de structure. *Ph.D. thesis, University Paris 6, France*

Mier, van, J.G.M. 1984. Strain-softening of concrete under multiaxial loading conditions, *PhD thesis, Technische Hogeschool Eindhoven.* https://doi.org/10.6100/IR145193

Montague, P. 1975. A simple Composite Construction for cylindricl shells subjected to external pressure. *Journal Mechanical Engineering Science* 17(2): 105–113. *https://doi.org/10.1243/JMES_JOUR_1975_017_016_02*

Oduyemi, T. & Wright, H. 1989. An Experimental Investigation into the Behaviour of Double-Skin Sandwich Beams. *J. Construct. Steel Research*, 14(3): 197–220. *https://doi.org/10.1016/0143-974X(89)90073-4*

Ollgaard, J.G., Slutter, R.G. & Fisher, J. 1971. Shear strength of stud connectors in lightweight and normal-weight concrete. *AISC Engineering Journal*, 8: 55–64.

Qin, F., Kong, Q., Li, M., Mo, Y L, Song G. & Fan, F. 2015. Bond slip detection of steel plate and concrete beams using smart aggregates. *Smart Materials and Structures* 24(11): *115039*. https://doi.org/10.1088/0964-1726/24/11/115039

Schlaseman, C. 2004. Application of Advanced Construction technologies to New Nuclear Power Plants. *MPR-2610, prepared for the US Department of Energy under contract for DE-AT01-02NE23476. https://www.nrc.gov/docs/ML0931/ML093160836.pdf*

Sener, K. C., Varma, A. H. & Seo, J. 2016. Experimental and numerical investigation of the shear behavior of steel-plate composite (SC) beams without shear reinforcement. *Engineering Structures.* 127: 495–509. https://doi.org/10.1016/j.engstruct.2016.08.053

Varma, A.H., Malushte, S.R. & Lai Z. 2015. Modularity & Innovation using steel-concrete-steel composite (SC) walls for nuclear and commercial construction, *Advances in Steel-Concrete Composite Structures, Proc 11th International Conference*, *Beijing, China, 3-5 December 2015. https://doi.org/10.13140/RG.2.1.4665.4804*

Wright, H.D., Oduyemi T.O.S. & Evans H.R. 1991. The experimental behavior of double skin composite elements. *Journal of Constructional Steel Research* 19(2): 97–110. *https://doi.org/10.1016/0143-974X(91)90036-Z*

Yan, J.-B., Liew, J. R., Zhang, M.H. & Wang, J. 2014. Ultimate strength behavior of steel-concrete-steel sandwich beams with ultra-lightweight cement composite, Part 1: Experimental and analytical study. *Steel and Composite Structures* 17(6): 907–927. *http://dx.doi.org/10.12989/scs.2014.17.6.907*

Yan, J.-B., Liew, J. R., Zhang, M.-H. & Sohel, K. 2015. Experimental and analytical study on ultimate strength behavior of steel-concrete-steel sandwich composite beam structures. *Materials and Structures* 48: 1523–1544. *https://doi.org/10.1617/s11527-014-0252-4*

Zhang, W. Huang, Z., Fu, Z., Qian, X., Zhou, Y. & Sui, L. 2020. Shear resistance behavior of partilly composite Steel-Concrete-Steel sandwich beams considering bond-slip effect. *Engineering Structures,* 210: 110394. *https://doi.org/10.1016/j.engstruct.2020.110394*